

A Bayesian Approach to Comparing Cosmic Ray Energy Spectra

S.Y. BenZvi¹, B.M. Connolly², C.G. Pfendner¹, and S. Westerhoff¹

ABSTRACT

A common problem in ultra-high energy cosmic ray physics is the comparison of energy spectra. The question is whether the spectra from two experiments or two regions of the sky agree within their statistical and systematic uncertainties. We develop a method to directly compare energy spectra for ultra-high energy cosmic rays from two different regions of the sky in the same experiment without reliance on agreement with a theoretical model of the energy spectra. The consistency between the two spectra is expressed in terms of a Bayes factor, defined here as the ratio of the likelihood of the two-parent source hypothesis to the likelihood of the one-parent source hypothesis. Unlike other methods, for example χ^2 tests, the Bayes factor allows for the calculation of the posterior odds ratio and correctly accounts for non-Gaussian uncertainties. The latter is particularly important at the highest energies, where the number of events is very small.

Subject headings: cosmic rays — methods: statistical

1. Introduction

A century after Victor Hess's discovery of cosmic rays, it is still unclear where and how these particles are accelerated. Some of them reach energies above 10^{20} eV, well above the capabilities of man-made accelerators. (See Beatty & Westerhoff (2009) for a recent review.) Clues about the origin of these ultra-high energy cosmic rays comes from the study of the cosmic ray energy spectrum. While basically a simple power law over the entire range of measured energies from GeV to above EeV, the spectrum shows some important features that might hold the key to discovering and understanding the sources. The most relevant feature at the ultra-high energy end of the spectrum is the flux suppression above around 6×10^{19} eV caused by the interaction of cosmic ray primaries with the photons of the 2.7 K microwave background, the so-called Greisen-Zatsepin-Kuz'min (GZK) suppression (Greisen 1966; Zatsepin & Kuzmin 1966), predicted already in 1966 shortly after the discovery of the microwave background. Recently, a flux suppression at the highest energies, consistent with the GZK suppression, has been observed in data recorded by the High Resolution Fly's Eye experiment in Utah (Abbasi et al. 2008a) and the Pierre Auger Observatory in

¹Department of Physics, University of Wisconsin-Madison, Madison, WI 53706

²University of Pennsylvania, Philadelphia, PA 19104

Argentina (Abraham et al. 2008b). If this suppression is indeed the long-sought GZK suppression and not an intrinsic feature of the sources, we now know that most of the highest energy cosmic rays are produced at large distances. Those observed on Earth with energies above 6×10^{19} eV must originate from sources closer than 80 to 100 Mpc, or from within what is referred to as the “GZK sphere.”

The existence of a suppression at ultra-high energies is not all that can be learned from the energy spectrum. The exact shape of the spectrum in the GZK suppression region can provide information on the actual distribution of the sources. Furthermore, the energy spectrum is sensitive to a variety of factors, including production and transport mechanisms, and cosmic ray mass composition. Because of the sensitivity of the spectrum to these effects, it is useful to examine the spectrum in multiple ways. Experiments like the Pierre Auger Observatory and the Telescope Array experiment now collect data at an unprecedented rate, so several studies that were not possible years ago when the total number of detected events at the highest energies was little more than a handful, are now possible for the first time.

One possible study that may give some insight into the origin of cosmic rays is a comparison of the energy spectrum in different regions of the sky. The spectrum in a region that contains one or more strong cosmic ray sources can potentially deviate from the all-sky spectrum. If the source is closer than 80 Mpc, for example, its flux is not expected to show a GZK suppression. Recently, the region around the Active Galactic Nuclei (AGN) Centaurus A has been identified as a possible region of an enhanced cosmic ray flux in Auger data (Abraham et al. 2008a; Abreu et al. 2010). Since Cen A is nearby (4 Mpc), the energy spectrum in the Cen A region could differ from the all-sky cosmic ray energy spectrum.

More generally, increased statistics from the current generation of instruments will eventually allow a detailed comparison of the shape of the cosmic ray flux as a function of the sky position, thus creating a “skymap” of spectral parameters, for example of the spectral index. Such a study might reveal sky regions where cosmic ray accelerators are located. For this study to be as general as possible, it should not be limited to comparing power law indices, as the spectrum in certain parts of the sky might not be well described by a power law or even a broken power law. An ideal method would compare the shape of the spectrum in a certain region of the sky to the all-sky flux without any prejudice as to the functional form of the spectrum.

An additional complication is the fact that measurements of the energy spectrum are often plagued by 20%-30% systematic uncertainties in energy measurement and low statistics at the highest energies. The measurements at the highest energy values are often determined by only a few events. A rigorous statistical analysis must therefore be applied to the spectra to compare them and extract any sort of meaning.

In this paper, we develop a statistical method to compare cosmic ray energy spectra. The method uses a Bayes factor formulation where the likelihood of the hypothesis that the two energy spectra stem from one source (the “one-parent” hypothesis) is compared to the likelihood of the

hypothesis that the spectra stem from different sources (the “two-parent” hypothesis).

There are several advantages to a Bayesian approach to model selection. Most importantly, it allows for the calculation of the posterior odds ratio in favor of the two-parent hypothesis over the one-parent hypothesis, which is the relevant model selection parameter. Unlike a χ^2 -test, it takes into account the alternative hypothesis, and it automatically penalizes over-fitting of the data with complex models. In contrast to a χ^2 - or F -test, it allows for non-Gaussian uncertainties in the data, a feature that is important in the comparison of cosmic ray energy spectra, as the number of events at the highest energies is very small. In addition, the Bayesian formalism allows for the marginalization of nuisance parameters and systematic uncertainties. Marginalization provides a convenient way to quantify our ignorance of nuisance parameters with the judicious choice of prior probability distributions.

We develop two different techniques for comparing the spectra. The first method compares the absolute flux of the spectra. This method depends on knowledge of the relative exposure of the two data sets. The second method is similar except that we remove the dependence on the known relative exposure and compare the spectra using no absolute scale; instead, we marginalize the relative weight (the scaling factor) of the spectra in the one-parent case. This lack of dependence on the relative exposure allows one to compare the shape of the spectra without comparing the absolute flux. This is useful in cases where the relative exposure between data sets is not known with sufficient accuracy, or when the absolute flux is not considered relevant in the comparison.

The paper is organized as follows. In Section 2, we develop the two methods to compare the energy spectra. In Section 3, we use simulated data to test the methods and evaluate their sensitivity. In Section 4, we compare the Bayes factor method to a χ^2 -test. The paper is summarized in Section 5.

2. Method

Let $\vec{\mathcal{F}}_1 = \{\mathcal{F}_{1,i}\}$ and $\vec{\mathcal{F}}_2 = \{\mathcal{F}_{2,i}\}$ be the (binned) observed fluxes that are to be compared. Then the Bayes factor B_{21} is the likelihood ratio that the measurements arise from two parent distributions versus a single parent distribution,

$$B_{21} = \frac{P(\vec{\mathcal{F}}_1, \vec{\mathcal{F}}_2 | H_2)}{P(\vec{\mathcal{F}}_1, \vec{\mathcal{F}}_2 | H_1)} \quad , \quad (1)$$

where H_1 and H_2 indicate the one- and two-parent hypothesis, respectively. The Bayes factor is equal to the posterior odds ratio

$$\frac{P(H_2 | \vec{\mathcal{F}}_1, \vec{\mathcal{F}}_2)}{P(H_1 | \vec{\mathcal{F}}_1, \vec{\mathcal{F}}_2)} = \frac{P(\vec{\mathcal{F}}_1, \vec{\mathcal{F}}_2 | H_2) P(H_2)}{P(\vec{\mathcal{F}}_1, \vec{\mathcal{F}}_2 | H_1) P(H_1)} = B_{21} \frac{P(H_2)}{P(H_1)} \quad , \quad (2)$$

commonly used in Bayesian model selection when $P(H_1) = P(H_2)$, *i.e.*, when the prior probabilities of the hypotheses in question are equivalent (Kass & Raftery 1995; Goodman 1999). In other

words, B_{21} is a quantity which derives solely from the data. It describes how the data will cause an experimenter to favor one or another hypothesis after conducting an experiment, independent of prior beliefs or prejudices regarding the two hypotheses.

Because it is a ratio, B_{21} can take on any value between 0 and ∞ . To make sense of its value, it is convenient to note the connection between the Bayes factor and the posterior probability. For example, if we do not favor either model before taking data ($P(H_1) = P(H_2)$), we can use Bayes’ Theorem to express the posterior probability of the null (one-parent) hypothesis purely in terms of the Bayes factor:

$$P(H_1|\vec{\mathcal{F}}_1, \vec{\mathcal{F}}_2) = \frac{1}{1 + B_{21}} \quad (3)$$

A Bayes factor $B_{21} = 10^{-2}$ indicates that the posterior probability of the one-parent hypothesis given the data is 99%; and $B_{21} = 10^2$ indicates that the posterior probability is 0.99%. Hence, it is conventional to interpret $B_{21} > 10^2$ as strong or decisive evidence against the null hypothesis, and $B_{21} < 10^{-2}$ as decisive evidence in favor of the null hypothesis (Jeffreys 1939). Of course, it is possible to adjust these decision thresholds according to one’s needs. If it is preferable to use the “5-sigma” convention of overwhelming evidence, the necessary limits on the Bayes factor can be computed using Eq. (3), assuming there are no prior prejudices toward H_1 or H_2 .

In this calculation, we compare the observed fluxes $\vec{\mathcal{F}}_1$ and $\vec{\mathcal{F}}_2$ with the expected values $\vec{f}_1 = \{f_{1,i}\}$ and $\vec{f}_2 = \{f_{2,i}\}$ given a particular hypothesis. It is convenient to express the expectation in terms of the total expected counts $\{\eta_i\}$ and a set of weights $\{w_i\}$ such that

$$f_{1,i} = w_i\eta_i, \quad f_{2,i} = (1 - w_i)\eta_i . \quad (4)$$

The weights have values between 0 and 1 and the counts can take on any positive value. Since the expected fluxes \vec{f}_1 and \vec{f}_2 are unknown, we marginalize these parameters in the Bayes factor, so Eq. 1 becomes

$$B_{21} = \frac{\int \int P(\vec{\mathcal{F}}_1, \vec{\mathcal{F}}_2|\vec{f}_1, \vec{f}_2, H_2)P(\vec{f}_1, \vec{f}_2|H_2)d\vec{f}_1d\vec{f}_2}{\int \int P(\vec{\mathcal{F}}_1, \vec{\mathcal{F}}_2|\vec{f}_1, \vec{f}_2, H_1)P(\vec{f}_1, \vec{f}_2|H_1)d\vec{f}_1d\vec{f}_2} \quad (5)$$

$$= \frac{\int \int P(\vec{\mathcal{F}}_1, \vec{\mathcal{F}}_2|\vec{w}', \vec{\eta}, H_2)P(\vec{w}', \vec{\eta}|H_2)d\vec{w}'d\vec{\eta}}{\int \int P(\vec{\mathcal{F}}_1, \vec{\mathcal{F}}_2|\vec{w}, \vec{\eta}, H_1)P(\vec{w}, \vec{\eta}|H_1)d\vec{w}d\vec{\eta}} . \quad (6)$$

Method A and B now differ in the treatment of the weights w_i for the one- and two-parent hypotheses. These prior model restrictions on the weights can be introduced via the probabilities $P(\vec{f}_1, \vec{f}_2|H_1)$ and $P(\vec{f}_1, \vec{f}_2|H_2)$.

2.1. Method A: Comparing Absolute Flux

In method A, in the one-parent hypothesis, the weights are simply the (known) relative exposure for the two data sets:

$$w_i = \frac{(\text{Exposure}_1)_i}{(\text{Exposure}_1)_i + (\text{Exposure}_2)_i} . \quad (7)$$

In the denominator of Eq. 6, the marginalization over the weights w_i therefore collapses since we equate the weights with the relative experimental exposures. In the two-parent hypothesis, every possible relative exposure is allowed since the absolute flux in the two regions could be different. Therefore, each of the weights are allowed to take on any value between 0 and 1.

We treat the error in the flux as Poissonian, so the probability $P(\vec{\mathcal{F}}_1, \vec{\mathcal{F}}_2 | w, \eta)_i$ of observing counts $\{\mathcal{F}_{1,i}\}$ and $\{\mathcal{F}_{2,i}\}$ given expected counts $\vec{f}_1 = \{w_i \eta_i\}$ and $\vec{f}_2 = \{(1 - w_i) \eta_i\}$ becomes

$$P(\mathcal{F}_1, \mathcal{F}_2 | w, \eta)_i = \frac{(w_i \eta_i)^{\mathcal{F}_{1,i}} e^{-w_i \eta_i}}{\mathcal{F}_{1,i}!} \frac{((1 - w_i) \eta_i)^{\mathcal{F}_{2,i}} e^{-(1-w_i) \eta_i}}{\mathcal{F}_{2,i}!} , \quad (8)$$

thus the Bayes factor is

$$B_{21} = \frac{\prod_{i=1}^N \int_0^1 dw_i \int_0^\infty d\eta_i \frac{(w_i \eta_i)^{\mathcal{F}_{1,i}} e^{-w_i \eta_i}}{\mathcal{F}_{1,i}!} \frac{((1-w_i) \eta_i)^{\mathcal{F}_{2,i}} e^{-(1-w_i) \eta_i}}{\mathcal{F}_{2,i}!}}{\prod_{i=1}^N \int_0^\infty d\eta_i \frac{(w_i \eta_i)^{\mathcal{F}_{1,i}} e^{-w_i \eta_i}}{\mathcal{F}_{1,i}!} \frac{((1-w_i) \eta_i)^{\mathcal{F}_{2,i}} e^{-(1-w_i) \eta_i}}{\mathcal{F}_{2,i}!}} , \quad (9)$$

where N is the number of bins. Note that a flat prior $P(\eta_i | H) = 1/(\eta_{\max} - \eta_{\min})$ for η_i is actually improper in the limit $\eta_{\min} = 0$ and $\eta_{\max} \rightarrow \infty$. The problem can be circumvented by explicitly using η_{\min} and η_{\max} and letting them go to zero and infinity only after integration (Jaynes & Bretthorst 2003). In our example, the η_i -dependence actually cancels out.

Rearranging the Bayes factor, one gets

$$B_{21} = \frac{\prod_{i=1}^N \int_0^1 dw_i w_i^{\mathcal{F}_{1,i}} (1 - w_i)^{\mathcal{F}_{2,i}} \int_0^\infty d\eta_i e^{-\eta_i} \eta_i^{\mathcal{F}_{1,i} + \mathcal{F}_{2,i}}}{\prod_{i=1}^N w_i^{\mathcal{F}_{1,i}} (1 - w_i)^{\mathcal{F}_{2,i}} \int_0^\infty d\eta_i e^{-\eta_i} \eta_i^{\mathcal{F}_{1,i} + \mathcal{F}_{2,i}}} . \quad (10)$$

Since the η_i terms cancel, this reduces to

$$B_{21} = \frac{\prod_{i=1}^N \int_0^1 dw_i w_i^{\mathcal{F}_{1,i}} (1 - w_i)^{\mathcal{F}_{2,i}}}{\prod_{i=1}^N w_i^{\mathcal{F}_{1,i}} (1 - w_i)^{\mathcal{F}_{2,i}}} . \quad (11)$$

Using the identity

$$\frac{\Gamma(a) \Gamma(b)}{\Gamma(a+b)} = \int_0^1 t^{a-1} (1-t)^{b-1} dt , \quad (12)$$

the Bayes factor can be written as

$$B_{21} = \frac{\prod_{i=1}^N \frac{\Gamma(\mathcal{F}_{1,i}+1) \Gamma(\mathcal{F}_{2,i}+1)}{\Gamma(\mathcal{F}_{1,i}+\mathcal{F}_{2,i}+2)}}{\prod_{i=1}^N w_i^{\mathcal{F}_{1,i}} (1 - w_i)^{\mathcal{F}_{2,i}}} . \quad (13)$$

In our case, the \mathcal{F} terms are all positive integers, so the gamma functions reduce to factorials and we are left with the following form:

$$B_{21} = \frac{\prod_{i=1}^N \frac{\mathcal{F}_{1,i}! \mathcal{F}_{2,i}!}{(\mathcal{F}_{1,i}+\mathcal{F}_{2,i}+1)!}}{\prod_{i=1}^N w_i^{\mathcal{F}_{1,i}} (1 - w_i)^{\mathcal{F}_{2,i}}} . \quad (14)$$

For the purpose of calculation, it is more convenient to deal with the logarithm of the Bayes factor in Eq. 13,

$$\ln B_{21} = \sum_{i=1}^N \left[\ln(\Gamma(\mathcal{F}_{1,i} + 1)) + \ln(\Gamma(\mathcal{F}_{2,i} + 1)) - \ln(\Gamma(\mathcal{F}_{1,i} + \mathcal{F}_{2,i} + 2)) - \mathcal{F}_{1,i} \ln(w_i) - \mathcal{F}_{2,i} \ln(1 - w_i) \right]. \quad (15)$$

2.2. Method B: Comparing Shape of Spectrum Only

Next we want to compare the shape of the spectra without making any assumptions on the relative exposure. This is relevant in cases where we do not want the comparison to depend on an accurate knowledge of the exposure. The two-parent case remains the same as in method A, since we already allow every possible relative exposure. However, the one-parent hypothesis needs to be modified. We now allow the weights w_i to float, but not from bin to bin as in method A. Rather, we want the weight to act as a normalization factor to allow the spectra to scale together over all bins at once. The weights w_i are therefore not bin-dependent and can be described by a single weight $w = w_i$ which is allowed to float between 0 and 1.

The Bayes factor therefore now becomes

$$B_{21} = \frac{\prod_{i=1}^N \int_0^1 dw_i \int_0^\infty d\eta_i \frac{(w_i \eta_i)^{\mathcal{F}_{1,i}} e^{-w_i \eta_i}}{\mathcal{F}_{1,i}!} \frac{((1-w_i) \eta_i)^{\mathcal{F}_{2,i}} e^{-(1-w_i) \eta_i}}{\mathcal{F}_{2,i}!}}{\int_0^1 dw \prod_{i=1}^N \int_0^\infty d\eta_i \frac{(w \eta_i)^{\mathcal{F}_{1,i}} e^{-w \eta_i}}{\mathcal{F}_{1,i}!} \frac{((1-w) \eta_i)^{\mathcal{F}_{2,i}} e^{-(1-w) \eta_i}}{\mathcal{F}_{2,i}!}}}. \quad (16)$$

Again, the η_i terms cancel and B_{21} reduces to

$$B_{21} = \frac{\prod_{i=1}^N \int_0^1 dw_i w_i^{\mathcal{F}_{1,i}} (1 - w_i)^{\mathcal{F}_{2,i}}}{\int_0^1 dw w^{\sum_{i=1}^N \mathcal{F}_{1,i}} (1 - w)^{\sum_{j=1}^N \mathcal{F}_{2,j}}}. \quad (17)$$

Since the sums $\sum_{i=1}^N \mathcal{F}_{1,i}$ and $\sum_{i=1}^N \mathcal{F}_{2,i}$ are simply the total number of events N_1 and N_2 in spectrum 1 and 2, this becomes

$$B_{21} = \left(\prod_{i=1}^N \frac{\Gamma(\mathcal{F}_{1,i} + 1) \Gamma(\mathcal{F}_{2,i} + 1)}{\Gamma(\mathcal{F}_{1,i} + \mathcal{F}_{2,i} + 2)} \right) \frac{\Gamma(N_1 + N_2 + 2)}{\Gamma(N_1 + 1) \Gamma(N_2 + 1)}, \quad (18)$$

which simplifies to

$$B_{21} = \left(\prod_{i=1}^N \frac{\mathcal{F}_{1,i}! \mathcal{F}_{2,i}!}{(\mathcal{F}_{1,i} + \mathcal{F}_{2,i} + 1)!} \right) \frac{(N_1 + N_2 + 1)!}{N_1! N_2!}. \quad (19)$$

As before, we actually the logarithm of the Bayes factor in Eq. 18,

$$\ln B_{21} = \sum_{i=1}^N \left[\ln(\Gamma(\mathcal{F}_{1,i} + 1)) + \ln(\Gamma(\mathcal{F}_{2,i} + 1)) - \ln(\Gamma(\mathcal{F}_{1,i} + \mathcal{F}_{2,i} + 2)) \right] + \ln(\Gamma(N_1 + N_2 + 2)) - \ln(\Gamma(N_1 + 1)) - \ln(\Gamma(N_2 + 1)). \quad (20)$$

3. Sensitivity

In this section, we evaluate the sensitivity of the methods by applying them to simulated spectra. We start with a few simple examples, comparing single power law spectra with different spectral indices, and single and broken power laws. These examples are meant to illustrate the general behavior of the Bayes factor. We will then study the sensitivity of the methods for more realistic scenarios, for example for an analysis that compares the energy spectrum in the region around a potential source to the all-sky cosmic ray energy spectrum. Several features of the spectra we compare in this section will closely resemble the shape of the most recent published energy spectrum of the Pierre Auger Observatory (Abraham et al. 2010). To summarize, the spectrum exhibits two main features, the “ankle” at $\log(E_{\text{ankle}}/\text{eV}) = 18.61 \pm 0.01$, and the onset of a flux suppression at $\log(E_{\text{br}}/\text{eV}) = 19.46 \pm 0.03$. At the ankle, the energy spectrum flattens from a spectral index of $\gamma_1 = 3.26 \pm 0.04$ to $\gamma_2 = 2.59 \pm 0.02$. At the suppression, the spectrum steepens again to a spectral index $\gamma_3 = 4.3 \pm 0.2$. The data is binned in 20 bins from $\log(E/\text{eV}) = 18.4$ to $\log(E/\text{eV}) = 20.4$. In this paper, we focus on the energy spectrum above the ankle, which contains 14519 events recorded with the surface detector array.

As described in the previous section, a Bayes factor $B_{21} > 1$ indicates that the two-parent hypothesis is supported, but only larger Bayes factors $B_{21} > 10$ or $B_{21} > 10^2$ provide substantial or decisive evidence against the one-parent hypothesis. Here, we will typically require the Bayes factor to exceed $B_{21} > 10^2$, considering the region $10^{-2} < B_{21} < 10^2$ as an “undecided” region, *i.e.*, a region where the evidence is too weak to come to a conclusion for or against the two-parent hypothesis.

For the following studies, we simulate power law spectra assuming Poissonian errors on the number of events per energy bin. As described in Section 2, we calculate the Bayes factor based on the number of events per energy bin, N_i , rather than the flux per energy bin. The spectral indices for the number of events N versus energy and flux versus energy differ by 1, so a spectral index of $\gamma = 2.7$ for the flux (roughly the measured all-sky value) corresponds to an index of 1.7 for the number of events.

3.1. Comparing Two Single Power Law Spectra

We first compare two simulated power law spectra with spectral indices γ_1 and γ_2 , respectively. The ability of any method to separate two spectra with a difference $\Delta\gamma = \gamma_2 - \gamma_1$ in spectral indices will depend on the number of events in each data set. To illustrate the general behavior of the Bayes factor, we first compare two simulated data sets of equal size N , but different spectral indices. The spectral index of the first data set is $\gamma_1 = 2.7$, and the spectral index of the second data set is γ_2 . Fig. 1 shows the Bayes factor B_{21} as a function of the difference $\Delta\gamma = \gamma_2 - \gamma_1$ for three different data set sizes and both methods. For $\Delta\gamma = 0$, the two spectra are identical, and the Bayes factor takes on small values, indicating strong support for the one-parent hypothesis. As expected, the

support for the one-parent hypothesis is strongest for the largest data set size. For increasing and decreasing values of $\Delta\gamma$, the Bayes factor quickly rises, and a Bayes factor of $B_{21} > 100$, indicating significant evidence that the data sets have different spectral indices, is reached faster for the larger data sets. The difference in spectral indices that the methods can resolve decreases from about 0.5 for data sets with $N = 1000$ to 0.2 for data sets with $N = 10\,000$. To show the statistical error of the Bayes factor determination, here and in the following analyses, the calculation of the Bayes factor is performed for a large number of random implementations of the two data sets, and the plot shows the median Bayes factor and the band that contains 68% of the random implementations.

An important question is how small the difference $\Delta\gamma$ can be before the method can no longer differentiate between the two power spectra, *i.e.* before the Bayes factor drops below some minimum value. The smallest $\Delta\gamma$ that the method can resolve with B_{21} above the desired minimum value is a measure of its sensitivity. It depends on the size of the data sets, with larger data sets improving the sensitivity. It also depends on the desired minimum Bayes factor, *i.e.* on the strength of the evidence against the one-parent hypothesis that the analyser requires. Fig. 2 shows the number of events necessary to reach Bayes factors $B_{21} = 100, 1000, \text{ and } 10\,000$ as a function of $\Delta\gamma$ for both methods. As an example, for a data set with 10,000 events in each set, the methods can resolve differences in $\Delta\gamma$ of less than 0.2. To reach a resolution of 0.15, around 15,000 events are necessary. For this analysis, the sensitivities for methods A and B are roughly identical.

3.2. Comparing a Single Power Law Spectrum to a Broken Power Law Spectrum

Another simple example is the comparison of two spectra where one is a single power law and the other is a broken power law. This is an example with important applications. If we assume that the spectral index of the second data set is identical to the index of the first data set for energies below some break energy E_{br} and different at energies above E_{br} , this example describes a scenario where a GZK-type suppression is present in one data set, but not in the other. This could potentially be the case for the comparison of the energy spectrum in the vicinity of a strong source of ultra-high energy cosmic rays to the all-sky cosmic ray spectrum if the source is within the GZK sphere and its flux is not subject to a suppression.

We start with a simple comparison using two data sets of the same size. The first data set is a single power law with spectral index $\gamma_1 = 2.59$. The second data set is a broken power law with the same index γ_1 from the lowest energy bin $\log(E/\text{eV}) = 18.61$ to the break energy $\log(E_{\text{br}}/\text{eV}) = 19.46$, and a steeper index $\gamma_2 = 4.3$ above E_{br} . This shape corresponds to the spectrum measured by the Pierre Auger Observatory (Abraham et al. 2010).

The spectra are produced in such a way that the total number of events below E_{br} is identical for the two data sets, so the data sets differ (in the differential and integral number of events) only above E_{br} . Both data sets contain about 10000 events, but because it has more events at higher energies, the data set following the single power law contains about 200 events more.

The Bayes factor will depend on the energy range considered for the comparison. We consider the energy range from some lower energy threshold E_{\min} to the highest energies. Fig. 3 shows the Bayes factor as a function of the lower energy threshold E_{\min} . The Bayes factor increases with increasing E_{\min} and reaches a maximum. For method A, which compares the spectra in shape and in absolute flux, the maximum Bayes factor occurs at about $\log(E_{\min}/\text{eV}) = 19.6$, slightly above $\log(E_{\text{br}}/\text{eV}) = 19.46$. This behavior is expected, as the spectra below the break agree and therefore do not contribute to the Bayes factor. For method B, which compares shape only, the Bayes factor reaches its maximum at a lower energy, around $\log(E_{\min}/\text{eV}) = 19.2$, indicating that more data is necessary for method B to reach the maximum of discrimination power. This is not surprising; since method B examines shape only, it requires more low-energy bins to recognize a difference between the spectra. Method A relies in part on the relative exposure, which like the spectral index is different above $\log(E_{\text{br}}/\text{eV}) = 19.46$. After the maximum is reached, the Bayes factor decreases with E_{\min} as the data sets become smaller and can no longer be distinguished due to low statistics.

3.3. Prospects for Studies of the Spectrum as a Function of Sky Location

In the study of the spectrum from a region around a strong source, the two data sets to be compared will typically be unequal in size, reflecting the fact that a small sky region around the source position is compared to the rest of the sky. A realistic test should account for the difference in the sizes of the data sets. We repeat the previous analysis comparing a single power law to a broken power law, but now the total number of events N_{tot} is distributed unequally: the single power law, representing the source region, contains (as an example) 5% of all events, whereas the broken power law, representing the all-sky cosmic ray flux, contains 95% of all events.

The Bayes factor as a function of the lower energy threshold is shown in Fig. 4, with $N_{\text{tot}} = 14519$, for method A (upper plot) and method B (lower plot). We also show the results for a data set with twice (Fig. 5) and three times the number of events (Fig. 6) to illustrate the improvement expected for larger data sets within reach of Auger during its anticipated lifetime.

The analysis indicates that with the current data, only method A can discriminate between the two spectral shapes with a Bayes factor exceeding 100. As in the example discussed in Section 3.2, the Bayes factor reaches a peak value at energies slightly higher than E_{br} for method A, whereas method B requires more data below the break energy. The Bayes factor increases with the size of the data set, and for a data set of twice the published size, method B starts to reach Bayes factors above 100 on average. The Bayes factors increase to peak values of 10^{10} and 10^5 for method A and B, respectively, for data sets of three times the published size. The data recorded with the fully-operational Pierre Auger Observatory should reach this size within three to four years.

In reality, the region around the source will contain not only source events, but also background events whose energy distribution follows the all-sky energy spectrum. The fraction of background

events in the source bin is difficult to predict as the source flux is not known. To study the effect, we repeat the previous analysis assuming that a fraction of the events in the source bin are background, which we will refer to as the contamination level. A contamination level of 0 means that all events in the source bin are source events, and a contamination level of 1 means that all events are background events. Fig. 7 shows the maximum Bayes factor (scanned over E_{\min}) as a function of contamination level for $N_{\text{tot}} = 14519$, assuming that the source region contains 5 % of all events. Again, we also show the results for a data set twice and three times as large (Fig. 8 and Fig. 9, respectively).

The figures indicate that with current Auger statistics, method A can potentially differentiate spectra at a level of $B_{21} > 100$ if the contamination level is less than 25 %, whereas method B cannot differentiate the spectra for any level of contamination. For twice and three times the current data, method A can differentiate the spectra for contamination levels less than 47 % and 57 %, respectively, and method B for contamination levels of 11 % and 28 %, respectively. The difference in the discrimination power of the two methods is quite substantial, indicating the advantage provided by an accurate knowledge of the exposure to the source region.

The Pierre Auger Observatory is scheduled to take data for at least another decade. Our studies suggest that in the next few years, as the data increase, the methods presented here will reach a sensitivity that enables us to study differences in the spectral shape as a function of sky position. A study of the region around a potential source could reveal significant differences in the energy spectrum compared to the rest of the sky.

4. Comparison to a χ^2 Test

In this section, we compare the posterior probability of the one-parent hypothesis derived from the Bayesian analysis to the tail probability obtained from a straightforward two-sample χ^2 test. We use the simple example of the single and broken power law spectrum from Section 3.2. The χ^2 test statistic is

$$\chi^2 = \frac{1}{n_1 n_2} \sum_{i=1}^m \frac{(n_2 n_{1i} - n_1 n_{2i})^2}{n_{1i} + n_{2i}}, \quad (21)$$

where n_{1i} and n_{2i} are the counts for spectrum 1 and 2 in bin i , n_1 and n_2 are the total number of events in data set 1 and 2, and m is the number of bins (Fisher 1922). The statistic in Eq. 21 has approximately a χ_{m-1}^2 distribution for samples of sufficient size. Whether or not this requirement is met needs to be carefully checked for each application, in particular for the comparison of cosmic ray spectra at the high-energy tail where the number of events is bound to be small. Assuming that the statistic in Eq. 21 follows a χ_{m-1}^2 distribution, the p -value of the null hypothesis that the two spectra are the same above $\log(E/\text{eV}) = 18.61$ is $p = 4.4 \times 10^{-18}$.

Note that the χ^2 in Eq. 21 has scaling constants that adjust for unequally-sized data samples, so the appropriate Bayesian method for comparison is method B. It gives a probability of 9.6×10^{-12}

that the compared sets derive from the same parent spectrum.

The posterior probability and the χ^2 probability are plotted as a function of E_{\min} in Fig. 10. Both show the same general dependence of the probability on E_{\min} . At face value, the χ^2 test gives consistently lower probabilities for all choices of E_{\min} , which in turn implies that the χ^2 test can resolve smaller differences in the energy spectra. However, our studies show that this is due to the fact that the test statistic in Eq. 21 exhibits considerable deviations from the theoretical χ^2_{m-1} distribution because the necessary condition ($n_{1i} \gg 1$ and $n_{2i} \gg 1$ in each bin) is violated in the high-energy tail of the spectrum. Even for data sets ten times the size of the current Auger event sample, the statistics are not sufficient in the high-energy tail of the spectrum. As a result, the use of χ^2 inflates the significance of the difference between the sets, and the χ^2 test cannot be applied. The Bayes factor, which assumes Poisson uncertainties in all bins, is not affected by this problem and is therefore the appropriate statistical test for comparisons of energy spectra at the highest energies.

We also note that at least some of the difference between the χ^2 test results and the Bayesian method can be attributed to the fact that the Bayes factor gives a posterior probability, while the χ^2 gives a tail probability. Tail probabilities are known to be biased against the null hypothesis by a factor of at least 10 with respect to posteriors (Sellke et al. 2001).

5. Outlook

The study of the energy spectrum of ultra-high energy cosmic rays at different parts of the sky is a powerful tool to search for the sources of cosmic rays. It can supplement direct searches for the sources, which are typically based on the statistical analysis of the arrival direction distribution of cosmic rays. The direct searches have proven difficult and results are inconclusive so far, even with the size and quality of the current generation of cosmic ray detectors (Abreu et al. 2010; Abbasi et al. 2008b). However, the cosmic ray data set is quickly reaching a size where studies of the shape of the energy spectrum as a function of sky location can give additional insight into the location and nature of cosmic ray sources. The Bayesian method described in this paper has several advantages that are important for the comparison of spectra of ultra-high energy cosmic rays. It allows for the calculation of the posterior odds ratio in favor of the two-parent hypothesis over the one-parent hypothesis, and it allows for non-Gaussian uncertainties in the data.

An important future application for this analysis is the study of the energy spectrum in the vicinity of potential sources within the GZK sphere. With a data set of about two to three times the size of the last published Auger data set, the Bayes factor method developed here is sensitive to the difference between the all-sky cosmic ray energy spectrum and an unattenuated power law spectrum expected if the source spectrum shows no intrinsic cutoff.

This work is supported by the National Science Foundation under contract number NSF-PHY-

0855300.

REFERENCES

- Abbasi, R. U., et al. 2008a, *Phys. Rev. Lett.*, 100, 101101
- . 2008b, *Astropart. Phys.*, 30, 175
- Abraham, J., et al. 2008a, *Astropart. Phys.*, 29, 188
- . 2008b, *Phys. Rev. Lett.*, 101, 061101
- . 2010, *Phys. Lett.*, B685, 239
- Abreu, P., et al. 2010, *Astropart. Phys.*, 34, 314
- Beatty, J. J., & Westerhoff, S. 2009, *Ann. Rev. Nucl. Part. Sci.*, 59, 319
- Fisher, R. 1922, *J. Roy. Stat. Soc.*, 85, 87
- Goodman, S. N. 1999, *Ann. Intern. Med.*, 130, 1005
- Greisen, K. 1966, *Phys. Rev. Lett.*, 16, 748
- Jaynes, E., & Bretthorst, G. 2003, *Probability Theory: The Logic of Science* (Cambridge University Press Cambridge:)
- Jeffreys, H. 1939, *Theory of probability*, 2nd edn. (Oxford University Press)
- Kass, R. E., & Raftery, A. E. 1995, *J. Am. Stat. Assoc.*, 90, 773
- Sellke, T., Bayarri, M., & Berger, J. 2001, *Am. Stat.*, 55, 62
- Zatsepin, G. T., & Kuzmin, V. A. 1966, *JETP Lett.*, 4, 78

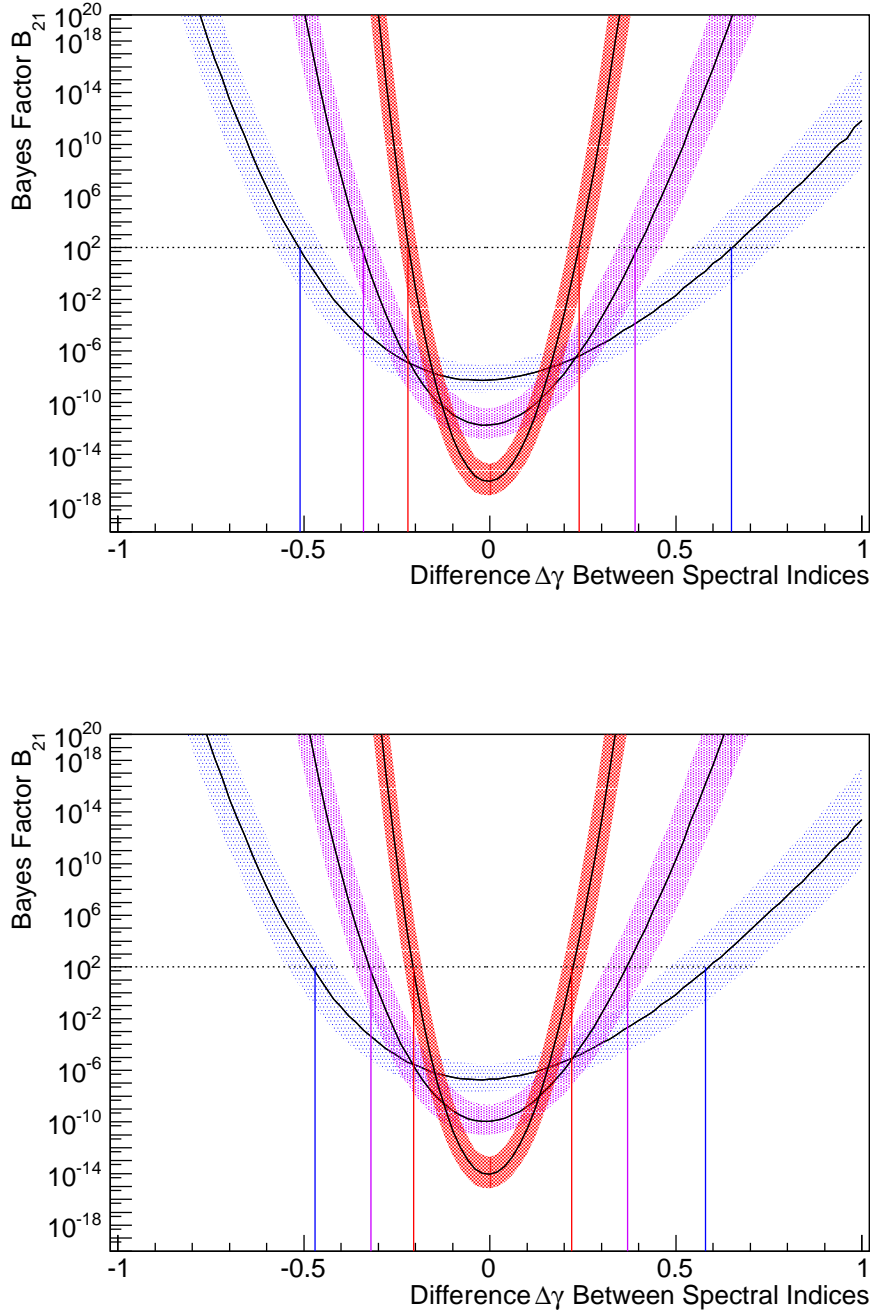


Fig. 1.— Bayes factor B_{21} as a function of difference in spectral index, $\Delta\gamma = \gamma_2 - \gamma_1$, for two power law spectra, analysed with method A (*top*) and method B (*bottom*). The spectral index of the first set is $\gamma_1 = 2.7$. The number of events in each set is 1000 (blue), 3000 (violet), and 10000 (red), and the shaded area represents the 68% error in each set. The analysis is performed for a large number of random implementations of the two data sets. The solid line indicates the median and the shaded area the 68% percentile. The horizontal line indicates a Bayes factor $B_{21} = 100$.

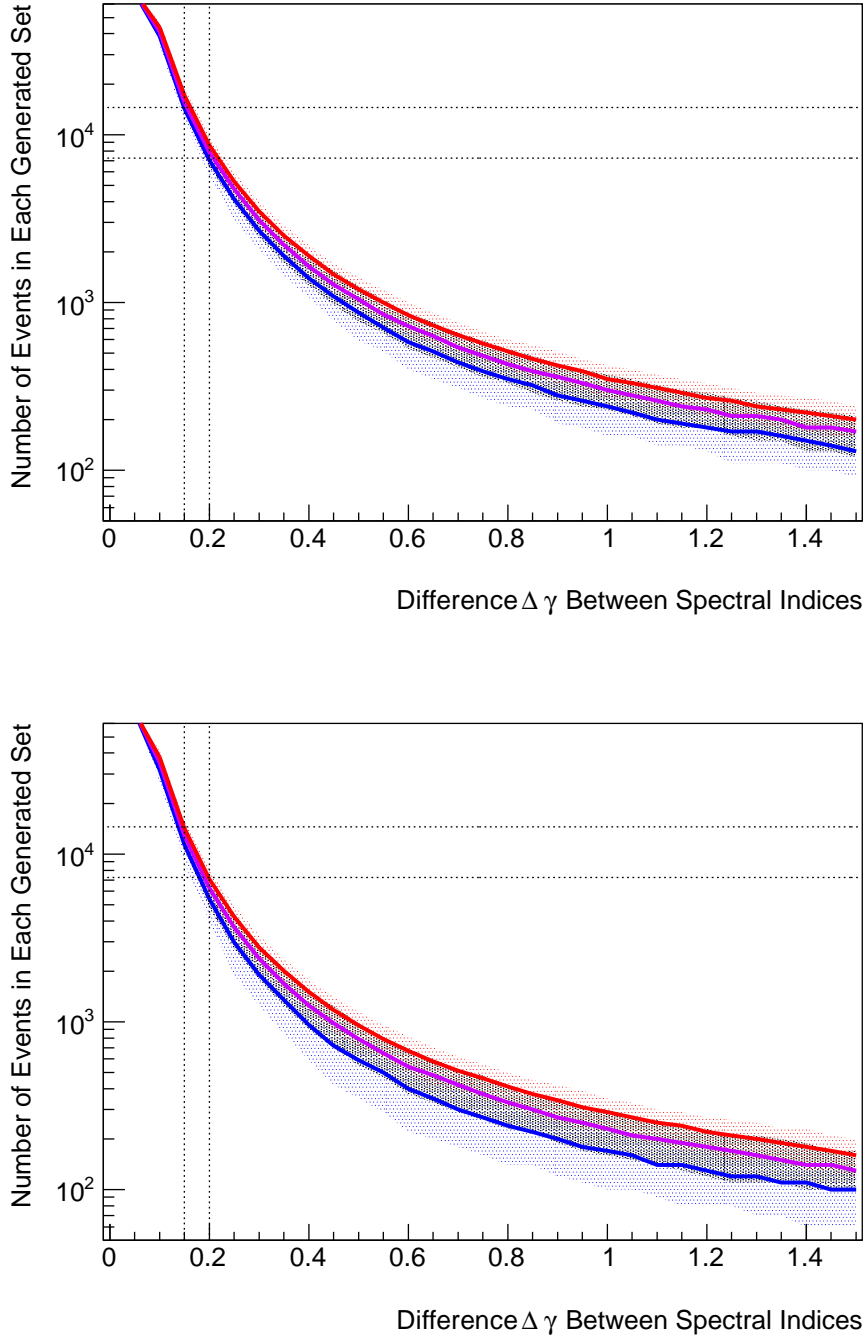


Fig. 2.— Number of events in each set required for two data sets representing single power laws with different spectral indices γ_1 and γ_2 so the Bayes factor B_{21} reaches 100 (blue), 1000 (violet), and 10 000 (red), as a function of the difference $\Delta\gamma = \gamma_2 - \gamma_1$ in spectral index. The spectral index of the first data set is fixed at $\gamma_1 = 2.7$. Results are shown for method A (*top*) and method B (*bottom*). The analysis is performed for a large number of random implementations of the two data sets. The solid line indicates the median and the shaded area the 68% percentile. The horizontal lines represent the number of events in the Auger data set and half that value. The vertical lines indicate differences in the power law index of 0.15 and 0.2.

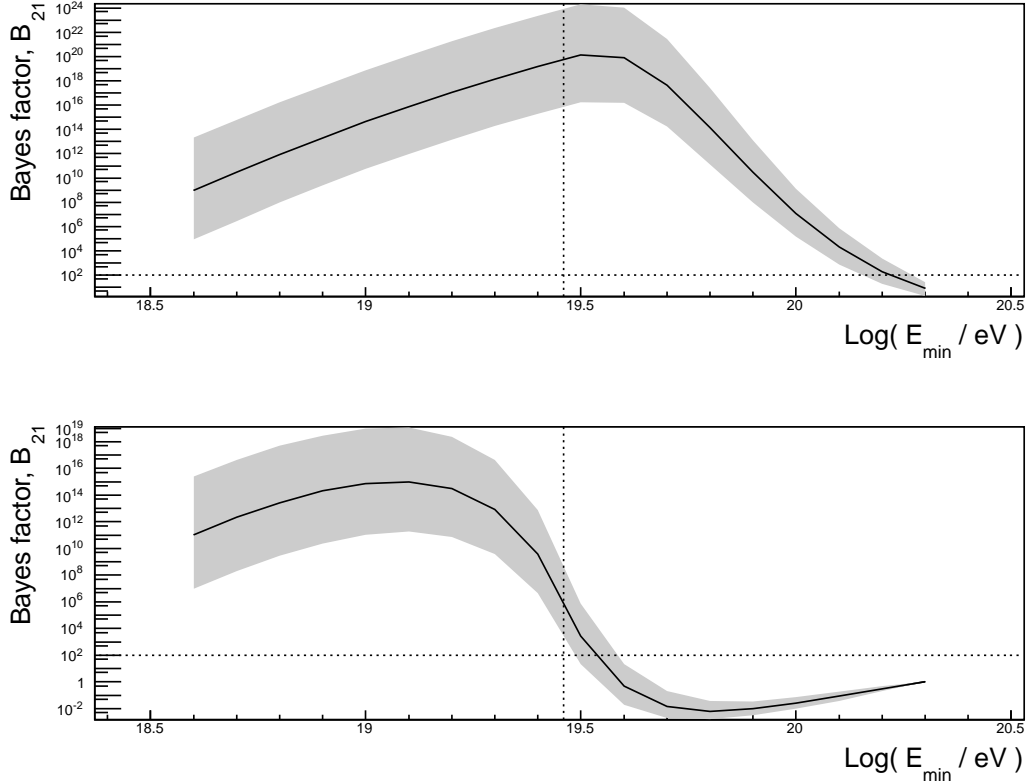


Fig. 3.— Bayes factor as a function of lower energy threshold E_{\min} for a comparison between a single power law and broken power law for method A (*top*) and B (*bottom*). The two spectra are identical within statistical errors for energies below $\log(E_{\text{br}}/\text{eV}) = 19.46$. Above E_{br} , the second data set steepens from $\gamma_1 = 2.59$ to $\gamma_2 = 4.3$. Each sets contains 10000 events. The analysis is performed for a large number of random implementations of the two data sets. The solid line indicates the median and the shaded area the 68 % percentile. The horizontal line indicates a Bayes factor $B_{21} = 100$. The vertical line indicates the position of the breakpoint in the broken power law at $\log(E_{\text{br}}/\text{eV}) = 19.46$.

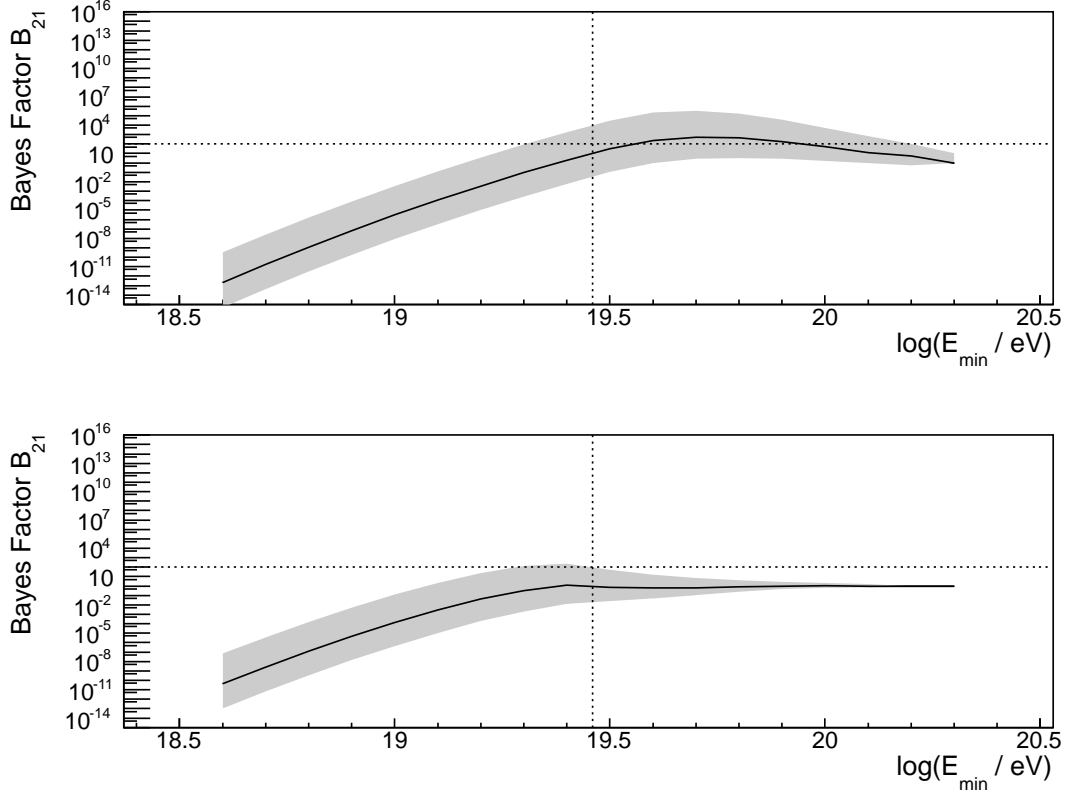


Fig. 4.— Bayes factor as a function of lower energy threshold E_{\min} for a comparison between a single power law and broken power law for method A (*top*) and B (*bottom*). The spectra have the same shape as in Fig. 3, but here, the total number of events in both sets is $N_{\text{tot}} = 14519$, with the broken power law data set containing $0.95 \times N_{\text{tot}}$ events and the single power law data set containing $0.05 \times N_{\text{tot}}$ events. The analysis is performed for a large number of random implementations of the two data sets. The solid lines indicate the median and the shaded area the 68% percentile. The horizontal line indicates a Bayes factor $B_{21} = 100$. The vertical line indicates the position of the breakpoint in the broken power law at $\log(E_{\text{br}}/\text{eV}) = 19.46$.

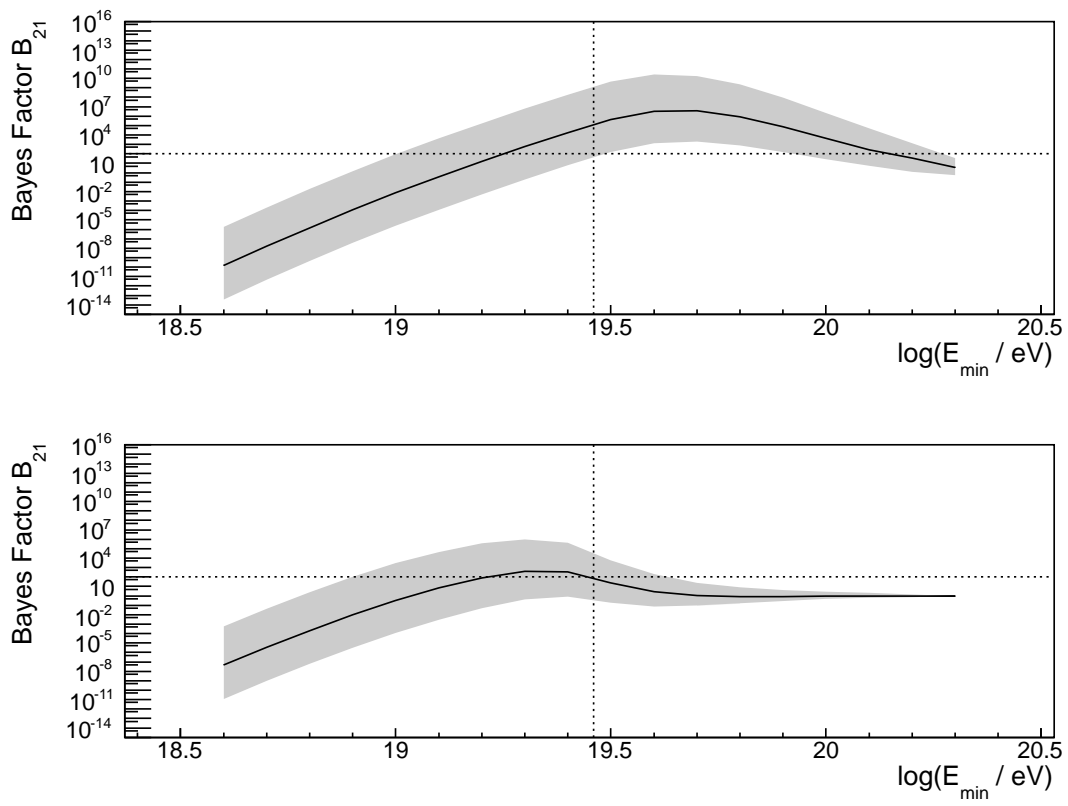


Fig. 5.— Same as Fig. 4, but for $N_{\text{tot}} = 29038$.

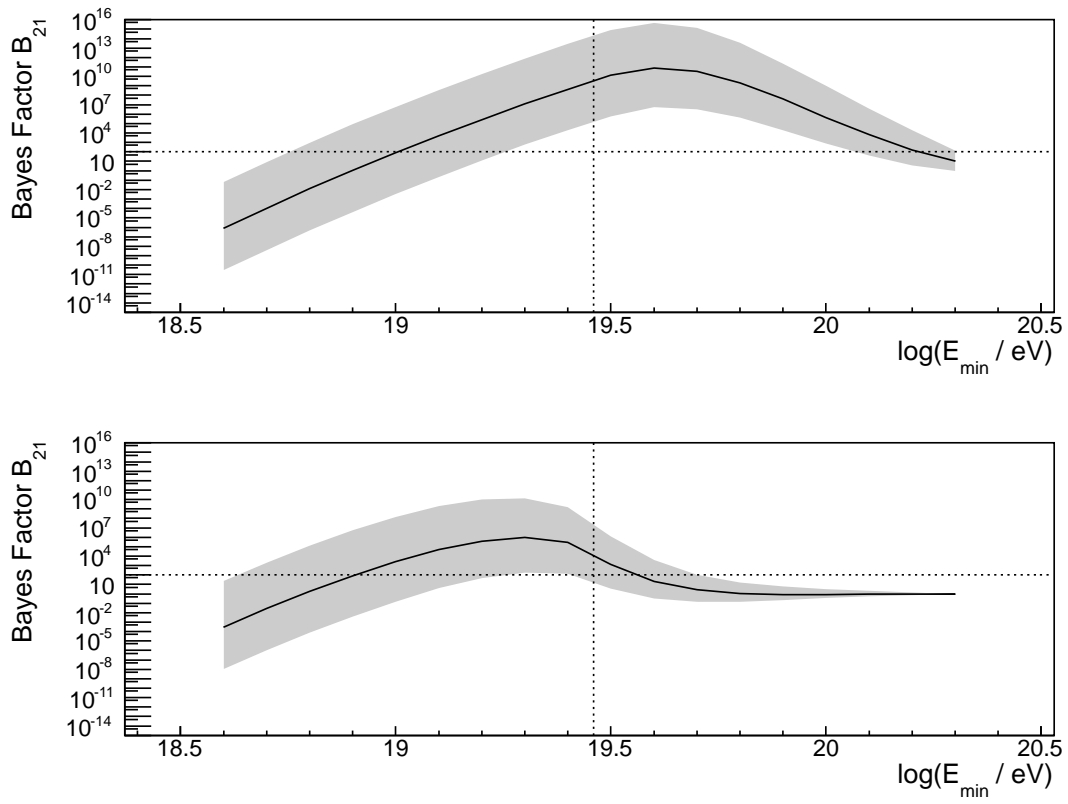


Fig. 6.— Same as Fig. 4, but for $N_{\text{tot}} = 43557$.

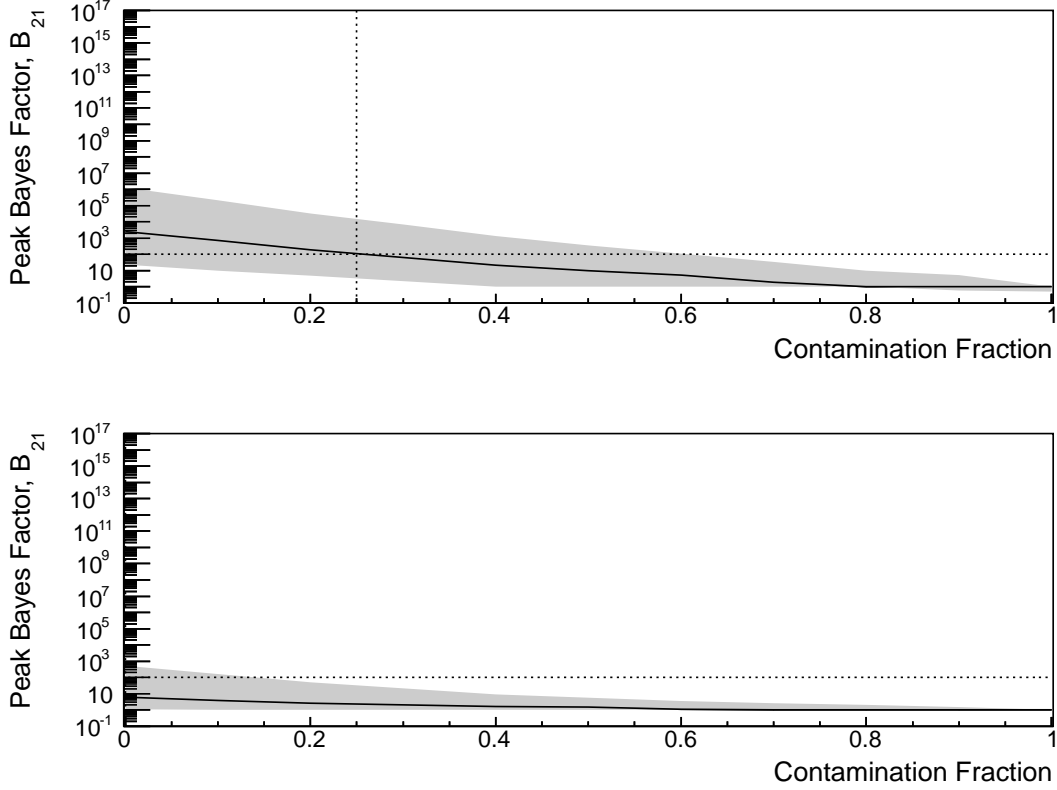


Fig. 7.— Peak Bayes factor as a function of the contamination fraction of a single power law source by the all-sky background broken power law spectrum for method A (*top*) and B (*bottom*). The spectra have the same shape as in Fig. 3. The total number of events is $N_{\text{tot}} = 14519$, with the broken power law data set containing $0.95 \times N_{\text{tot}}$ events and the single power law data set containing $0.05 \times N_{\text{tot}}$ events. The analysis is performed for a large number of random implementations of the two data sets. The solid lines indicate the median and the shaded area the 68% percentile. The horizontal line indicates a Bayes factor $B_{21} = 100$. The vertical line indicates the contamination fraction for which the median of the peak Bayes factor starts to exceed 100.

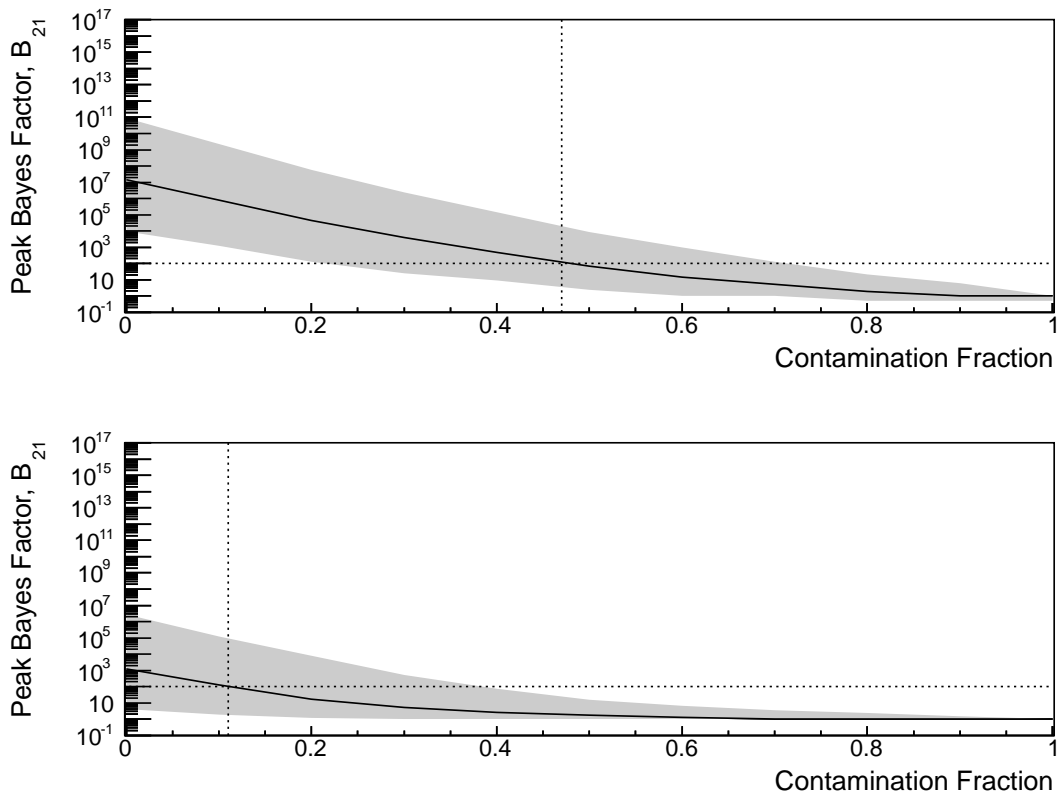


Fig. 8.— Same as Fig. 7, but for $N_{\text{tot}} = 29038$.

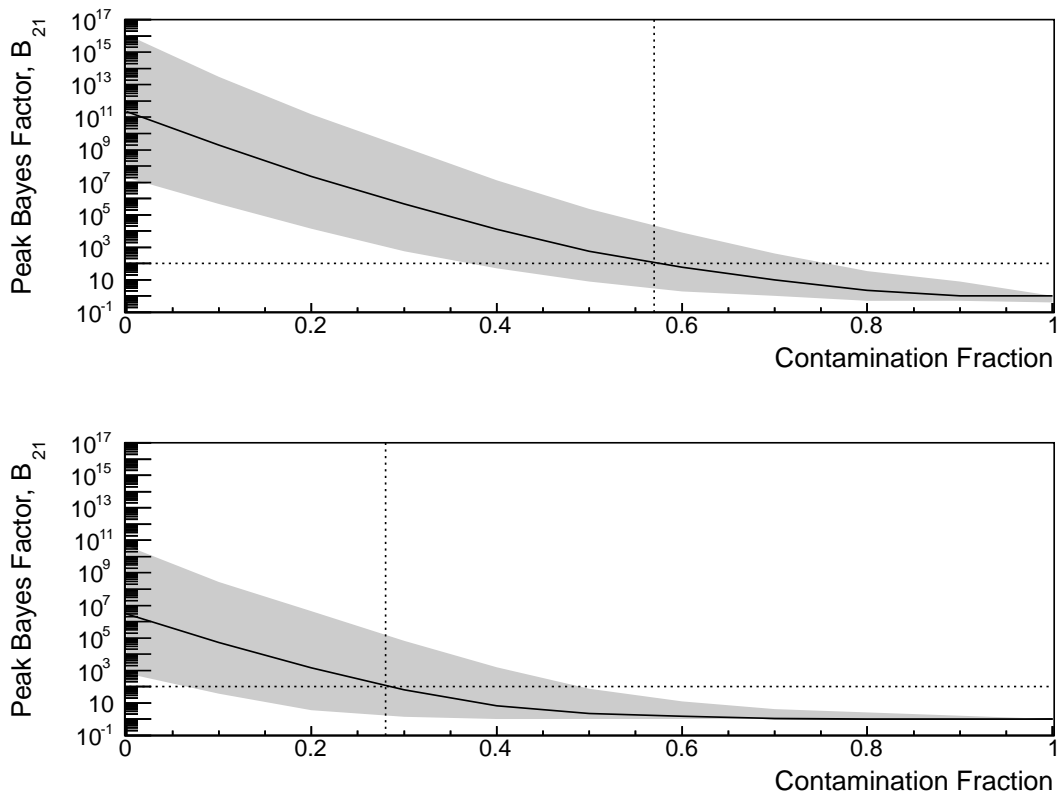


Fig. 9.— Same as Fig. 7, but for $N_{\text{tot}} = 43557$.

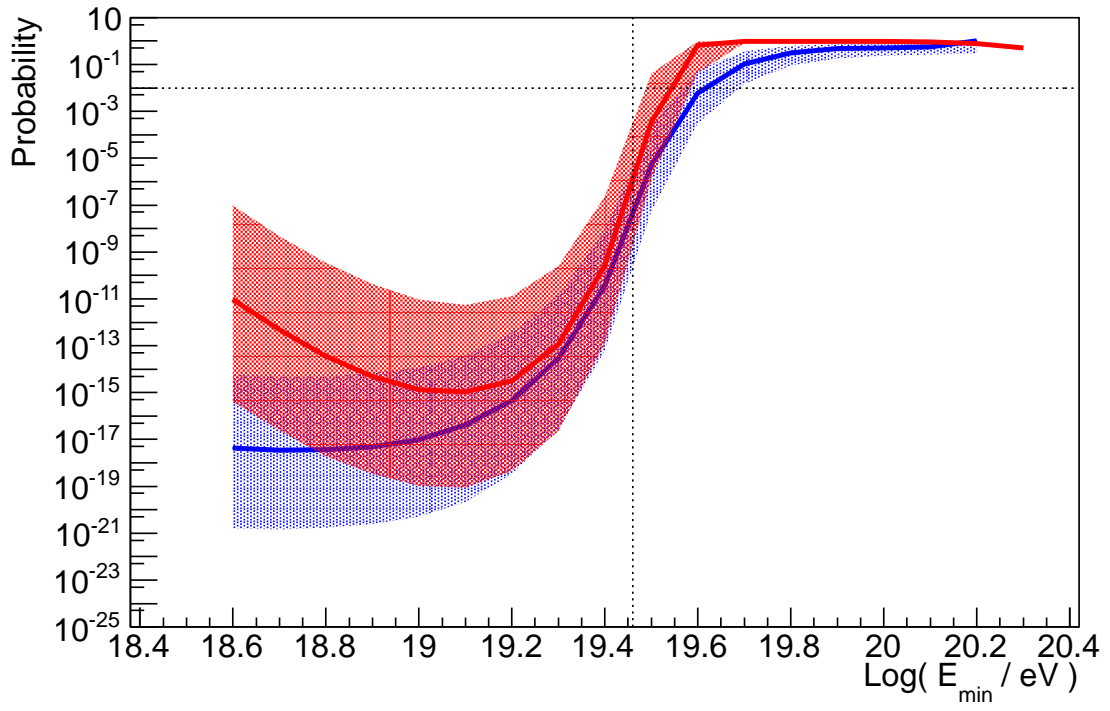


Fig. 10.— Posterior probability of the one-parent hypothesis (red), calculated using method B, and χ^2 probability (blue) as a function of the lower energy threshold E_{\min} for a comparison between a single power law and broken power law.